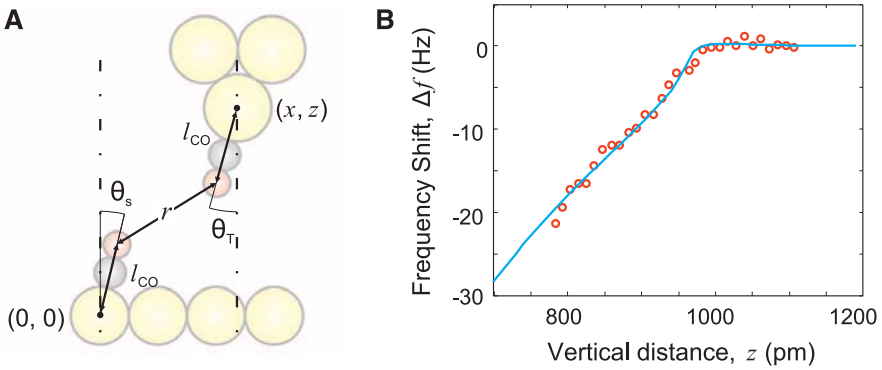

Fig. 3. Modeling the LFM process. (**A**) In our model, the final tip atom to which the CO is bound is set at (*x*, *z*). The tip CO molecule is allowed to relax by an angle θ_T, and the surface molecule is allowed to relax by an angle θ_S. (**B**) LFM data directly above the CO molecule as a function of vertical distance (*z*). Solid red points are experimental, and the blue curve is the calculated output.

that this value is much lower than that of the surface CO molecule. This lower value is expected because the apex of the tip does not present a full surface to the CO molecule, but rather a fraction thereof. The following conclusion can be drawn: The CO on the surface is laterally much stiffer and therefore a better probe. To increase the lateral stiffness of the tip, the CO molecule should be picked up on a blunt metal tip.

The LFM images have a strong signal that is much more spatially confined than are the normal-force AFM images. Physically, the spatial resolution of frequency-modulation AFM is limited by the lateral extent of the force gradient. Especially in the case of a CO-terminated tip—in which lateral forces change rapidly over a sharp transition, such as encountering an adsorbate—LFM increases the spatial resolution.

References and Notes

1. L. Gross, F. Mohn, N. Moll, P. Liljeroth, G. Meyer, *Science* **325**, 1110–1114 (2009).
2. F. Mohn, B. Schuler, L. Gross, G. Meyer, *Appl. Phys. Lett.* **102**, 073109 (2013).
3. J. Welker, F. J. Giessibl, *Science* **336**, 444–449 (2012).
4. J. Welker, A. J. Weymouth, F. J. Giessibl, *ACS Nano* **7**, 7377–7382 (2013).
5. D. M. Eigler, C. P. Lutz, W. E. Rudge, *Nature* **352**, 600–603 (1991).
6. L. Bartels, G. Meyer, K.-H. Rieder, *Appl. Phys. Lett.* **71**, 213 (1997).
7. N. Moll, L. Gross, F. Mohn, A. Curioni, G. Meyer, *New J. Phys.* **12**, 125020 (2010).
8. M. P. Boneschanscher *et al.*, *ACS Nano* **6**, 10216–10221 (2012).
9. J. Zhang *et al.*, *Science* **342**, 611–614 (2013).
10. N. Pavliček *et al.*, *Phys. Rev. Lett.* **108**, 086101 (2012).
11. F. Albrecht, M. Neu, C. Quest, I. Swart, J. Repp, *J. Am. Chem. Soc.* **135**, 9200–9203 (2013).
12. L. Gross *et al.*, *Science* **337**, 1326–1329 (2012).
13. Z. Sun, M. P. Boneschanscher, I. Swart, D. Vanmaekelbergh, P. Liljeroth, *Phys. Rev. Lett.* **106**, 046104 (2011).
14. M. Ternes *et al.*, *Phys. Rev. Lett.* **106**, 016802 (2011).
15. M. Ternes, C. P. Lutz, C. F. Hirjibehedin, F. J. Giessibl, A. J. Heinrich, *Science* **319**, 1066–1069 (2008).
16. O. Pfeiffer, R. Bennewitz, A. Baratoff, E. Meyer, P. Grütter, *Phys. Rev. B* **65**, 161403 (2002).
17. F. J. Giessibl, M. Herz, J. Mannhart, *Proc. Natl. Acad. Sci. U.S.A.* **99**, 12006–12010 (2002).
18. A. J. Weymouth *et al.*, *Phys. Rev. Lett.* **111**, 126103 (2013).
19. D. Rugar, R. Budakian, H. J. Mamin, B. W. Chui, *Nature* **430**, 329–332 (2004).
20. Materials and methods are available as supplementary materials on *Science* Online.
21. B. J. Albers *et al.*, *Nat. Nanotechnol.* **4**, 307–310 (2009).
22. J. E. Sader, S. P. Jarvis, *Appl. Phys. Lett.* **84**, 1801–1803 (2004).
23. J. Welker, E. Illek, F. J. Giessibl, *Beilstein J. Nanotechnol.* **3**, 238–248 (2012).
24. P. Morse, *Phys. Rev.* **34**, 57–64 (1929).
25. F. J. Giessibl, *Rev. Mod. Phys.* **75**, 949–983 (2003).
26. M. Gajdoš, J. Hafner, *Surf. Sci.* **590**, 117–126 (2005).
27. J. Braun *et al.*, *J. Chem. Phys.* **105**, 3258 (1996).

Acknowledgments: We thank D. Meuer for the LFM sensor construction, A.-K. Greitner for COMSOL modeling of the LFM sensor, and the Deutsche Forschungsgemeinschaft (GRK 1570) for financial support.

Supplementary Materials

www.sciencemag.org/content/343/6175/1120/suppl/DC1
Materials and Methods
Figs. S1 to S2

9 December 2013; accepted 23 January 2014
Published online 6 February 2014;
10.1126/science.1249502

Simultaneous Ground- and Space-Based Observations of the Plasmaspheric Plume and Reconnection

B. M. Walsh,[1,2]* J. C. Foster,[3] P. J. Erickson,[3] D. G. Sibeck[1]

Magnetic reconnection is the primary process through which energy couples from the solar wind into Earth's magnetosphere and ionosphere. Conditions both in the incident solar wind and in the magnetosphere are important in determining the efficiency of this energy transfer. In particular, the cold, dense plasmaspheric plume can substantially impact the coupling in the dayside reconnection region. Using ground-based total electron content (TEC) maps and measurements from the THEMIS spacecraft, we investigated simultaneous ionosphere and magnetosphere observations of the plasmaspheric plume and its involvement in an unsteady magnetic reconnection process. The observations show the full circulation pattern of the plasmaspheric plume and validate the connection between signatures of variability in the dense plume and reconnection at the magnetopause as measured in situ and through TEC measurements in the ionosphere.

The upward extension of cold, dense ionospheric plasma forms Earth's plasmasphere. The motion of the plasmaspheric particles is governed by two electric fields, resulting from corotation and convection motion. The first dominates close to Earth and enforces rotation of these particles with Earth. The second comes from solar wind–magnetosphere coupling, in response to the application of dawn-to-dusk solar wind electric fields to the magnetosphere and ionosphere. During geomagnetically quiet times, plasmaspheric particles on closed $\mathbf{E} \times \mathbf{B}$ drift shells maintain fairly steady populations. During disturbed times, the convection electric field increases, eroding the outer region of the plasmasphere into a drainage plume that extends sunward toward the dayside magnetopause (*1*, *2*) and noontime cusp ionosphere (*3*).

The spatial and temporal evolution of the plasmasphere-ionosphere plume can be measured through observations of total electron content (TEC) from ground-based Global Positioning Satellite (GPS) receivers. Integrated electron content is obtained through monitoring the phase delay of radio signals received from GPS spacecraft in circular orbits at an altitude of 20,000 km. These ground-based observations allow us to monitor the large-scale morphology and extent of the plasmaspheric plume (*4*). The structure and development of a sunward-extending plume in the dusk sector, as seen in TEC measurements, has been confirmed through extreme ultraviolet (EUV) imaging with NASA's IMAGE spacecraft (*3*); however, the sensitivity of these measurements does not allow for detection of plumes with lower densities and with large radial distances close to the magnetopause. Although the extension of the plume to the outer

[1]NASA Goddard Space Flight Center, Greenbelt, MD 20771, USA. [2]Space Sciences Laboratory, University of California, Berkeley, CA 94720, USA. [3]MIT Haystack Observatory, Westford, MA 01886, USA.

*Corresponding author. E-mail: brian.walsh@nasa.gov

magnetosphere has been inferred from ground-based and in situ measurements independently, coincident in situ spacecraft and ground-based measurements necessary to confirm the plume's full extension to the magnetopause and to the magnetic reconnection point have not been presented.

The presence of a high-density plasmaspheric plume at the reconnecting magnetopause is predicted to decrease the solar wind–magnetosphere coupling in the localized region of the plume (*5*–*8*). Through the process of magnetic reconnection, magnetic field lines in the solar wind interconnect with Earth's magnetospheric field lines, allowing plasma and energy to transfer from the solar wind into the magnetosphere and ionosphere. The efficiency of the reconnection process will govern how much energy is being transferred. Theory and simulations predict that the reconnection rate slows

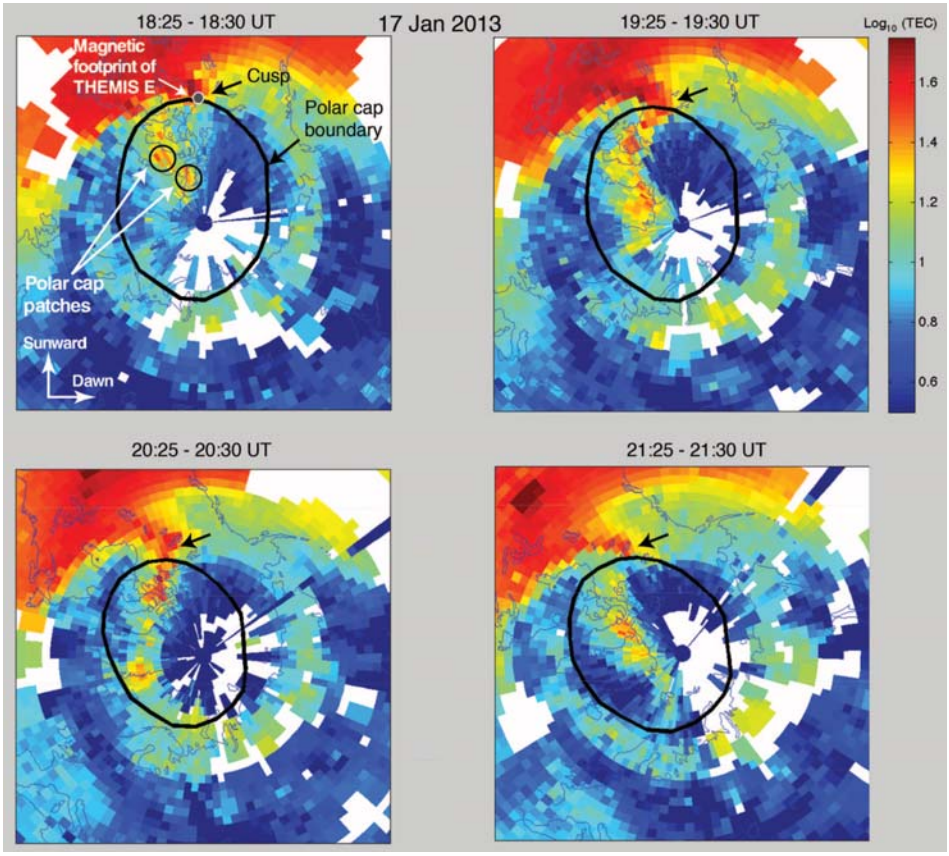

Fig. 1. GPS TEC maps showing temporal evolution of the SED plume at noontime cusp. The color scale shows TEC units (TECU) where 1 TECU = 10^{16} electrons/m^2. The plots are oriented so that local noon is up in each panel. The plume persists for a number of hours; the black arrow indicates the position of the cusp signature in the TEC data. The gray circle in the top left panel is the magnetic footprint of THEMIS E as it crosses the reconnecting magnetopause at 18:22 UT. The black circle is the poleward precipitation boundary from the OVATION model (*21*).

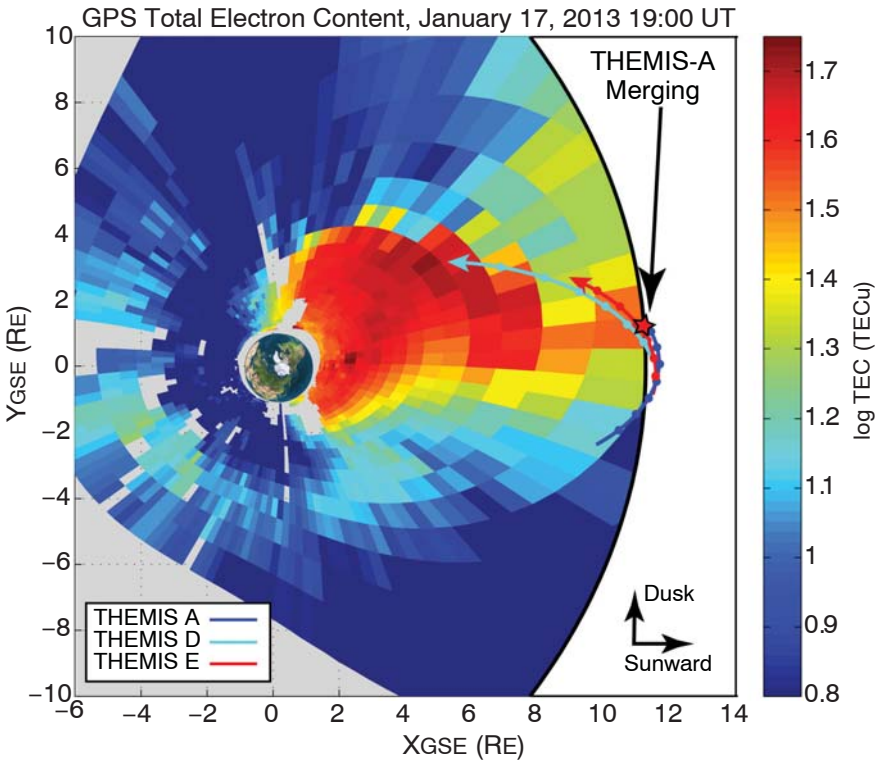

Fig. 2. TEC measurements projected to the equatorial plane following magnetic field lines with the International Geomagnetic Reference Field (IGRF) model. The star indicates the position where the THEMIS A spacecraft crosses the magnetopause. The solid circles along the orbit are each separated by 1 hour spanning the time period from 16 to 22 UT. The black line is a modeled position of the magnetopause (*22*).

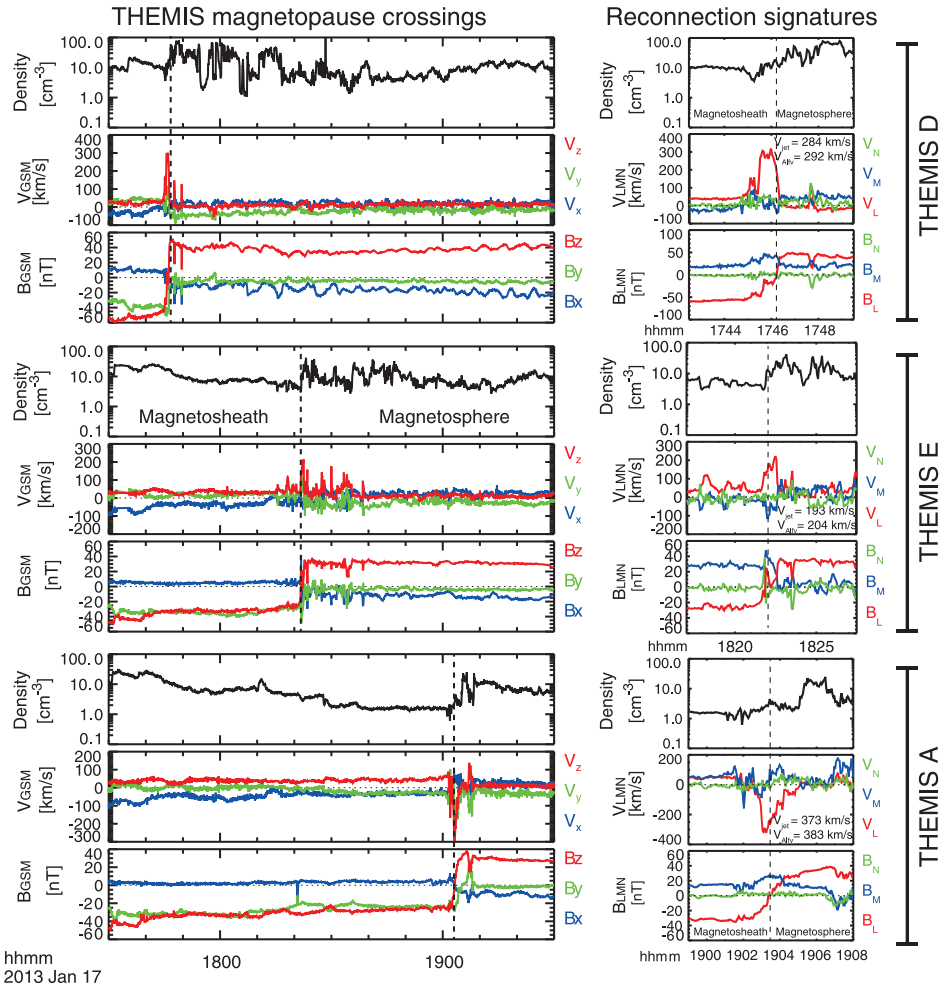

Fig. 3. Measurements from the three THEMIS spacecraft during each magnetopause crossing. The left plots show the same time scale for each spacecraft in GSM coordinates. The right plots are zoomed in on the time period of the magnetopause crossing and are in boundary normal (LMN) coordinates. For each spacecraft, the panels from top to bottom show electron density, bulk flow components, and magnetic field components. The LMN coordinate system is defined such that the N axis points outward along the magnetopause normal and the (L, M) plane is tangential to the magnetopause with L orientated due north and M due west. The vertical dashed black line indicates when each spacecraft passed through the magnetopause.

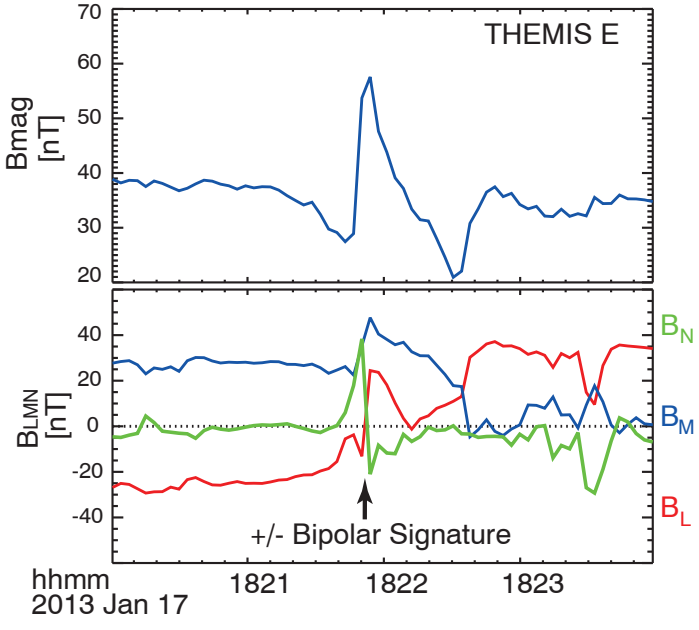

Fig. 4. Magnetic field measurements from THEMIS E during the magnetopause crossing in boundary normal coordinates. Clear signatures of a flux transfer event were observed. There is an enhancement in the magnetic field strength (top panel) corresponding to a bipolar signature in the B_N component and a deflection of the B_M component (bottom panel). Because the spacecraft is north of the reconnection site, as noted from the jets in the $+V_L$ direction (Fig. 3), an outward/inward (+, –) bipolar signature, indicating a northward-moving feature, is anticipated (*23*) and observed.

when the plasma density increases (*9*, *10*). Here we present simultaneous, magnetically coincident observations of the plume at the dayside reconnection point in both the magnetosphere and ionosphere.

On 17 January 2013, a coronal mass ejection (CME) impacted Earth's magnetosphere, resulting in a small geomagnetic storm, as indicated by the Disturbed Storm Time (*Dst*) index (minimum of –53 nT). During the storm, the ionospheric density increased and a long-duration storm-enhanced density (SED) plume (*11*) developed in TEC measurements (Fig. 1). The SED plume streamed in the convection flow from the dusk sector to the noontime cusp (arrow) and then antisunward across the polar cap, forming the polar tongue of ionization (TOI) (*12*). The patchy, intermittent structure of enhanced TEC within the TOI (Fig. 1) has been inferred to indicate variability in the rate of magnetopause reconnection (*13*, *14*).

During the same time period when the extended SED plume was monitored in the ionosphere, three of NASA's THEMIS spacecraft (*15*) detected the plume with in situ measurements at the magnetopause in a "string of pearls" formation (Fig. 2). The local time of the plume projected from the ionosphere is consistent with the location where THEMIS observed high-density plasma at the magnetopause (12.7 hours in magnetic local time), demonstrating the continuous extension of the plume from the inner magnetosphere sunward all the way to the magnetopause.

The THEMIS spacecraft were separated by roughly 45 min along the orbit. During the time plotted on the left in Fig. 3, each spacecraft passed from the magnetosheath into the magnetosphere. The magnetopause boundary is identified through a strong rotation in the *Z* magnetic field compo-

nent from –45 nT to 40 nT in the geocentric solar magnetospheric (GSM) coordinate system. This coordinate system is defined such that the X axis points from Earth to the Sun, Y is perpendicular to Earth's magnetic dipole axis so that the XZ plane contains the dipole axis, and Z is in the same sense as the northern magnetic pole. For each magnetopause crossing, the magnetospheric density adjacent to the magnetopause was greater than 10 cm^{-3}. This is close to two orders of magnitude greater than the nominal value, demonstrating the presence of a plume. The density was measured through the spacecraft potential.

During each of the three magnetopause crossings, a strong rotation of the magnetic field (>120°) and a reconnection jet were observed. These crossings provide several confirmations of magnetic reconnection and the participation of the dense plume in the process. The first confirmation is the jet velocity. The reconnection jet is caused by the magnetic tension force that accelerates the exhaust plasma to the Alfvén speed. In the case of asymmetric reconnection, when the density and magnetic field strength are not the same on both sides of the current sheet, the jet velocity is a hybrid of Alfvén speeds on both sides. In each boundary crossing, the jet velocity matches to within 5% of the predicted hybrid Alfvén speed (Fig. 3) as calculated by a previous model (*9*, *16*).

A second confirmation of the impact of the cold plume plasma is the location of the reconnection jet. Typically the magnetosheath is much denser than the dayside magnetosphere and the jet lies primarily on magnetic field lines with magnetospheric orientation ($+B_L$) (*17*, *18*). In our study, the region of the magnetosphere adjacent to the magnetopause has been mass-loaded and the jets are primarily on field lines with magnetosheath orientation ($-B_L$) (Fig. 3). The occurrence of reconnection jets primarily on field lines of magnetosheath orientation provides additional evidence for the impact of the plume density on magnetopause reconnection.

The location of THEMIS at the reconnecting magnetopause also maps to the point in the ionosphere where the TOI is formed and enhancements in TEC stream tailward over the pole on open field lines (Fig. 1). This confirms that the formation of the TOI in the ionosphere is spatially linked to the presence of the plume and reconnection at the magnetopause. The dense plasma on newly opened magnetic field lines convects tailward over the pole, as observed in the motion of TOI patches in the ionosphere and in situ at the magnetopause. Future studies using the high spatial and almost continuous coverage of the ground-based TEC maps may use this connection to monitor reconnection and identify when plume material has reached the magnetopause.

In addition to identifying substantial density enhancements and mass loading at the magnetopause, these conjugate measurements confirm the connection between intermittent reconnection signatures at the magnetopause and in the ionosphere. Bursts of reconnection can cause twisted magnetic flux ropes known as flux transfer events to form at the magnetopause (*19*, *20*). At the magnetopause, a flux transfer event, demonstrating intermittent or "bursty" reconnection, was observed in the THEMIS measurements (Fig. 4). In the ionosphere, patches of TEC enhancements known as polar cap patches were observed convecting over the pole on open magnetic field lines (Fig. 1). These patches correspond to variability in reconnection causing uneven rates of plasma to be transported over the pole. Previous work (*13*, *14*) used polar cap patches to infer variability in magnetopause reconnection; however, this association had not been validated through in situ measurements at the magnetopause.

Our results imply an extended plasmaspheric plume that spanned from a nominal plasmapause to the dayside magnetopause, where it impacted magnetic reconnection. Ground-based TEC measurements demonstrate that the extended plume existed for several hours. During this period, three THEMIS spacecraft provided magnetically coincident measurements of the plume mass-loading the magnetopause reconnection site near local noon. The spacecraft measurements show signatures of intermittent or bursty reconnection at the magnetopause corresponding to the occurrence of patches of enhanced TEC convecting tailward on open field lines over the pole in the ionosphere. The simultaneous observation of the conjugate location of the reconnection site at the magnetopause with the TEC cusp signature ionosphere (Fig. 1) is important. With this association validated, studies of the occurrence, location, and variability of reconnection at the magnetopause can be conducted with the assistance of ground-based TEC maps that provide high spatial and almost continuous temporal coverage.

References and Notes

1. C. R. Chappell, K. K. Harris, G. W. Sharp, *J. Geophys. Res.* **75**, 50–56 (1970).
2. C. R. Chappell, K. K. Harris, G. W. Sharp, *J. Geophys. Res.* **76**, 7632–7647 (1971).
3. J. C. Foster, A. J. Coster, P. J. Erickson, F. J. Rich, B. R. Sandel, *Geophys. Res. Lett.* **31**, L08809 (2004).
4. J. C. Foster, P. J. Erickson, A. J. Coster, J. Goldstein, F. J. Rich, *Geophys. Res. Lett.* **29**, 1623 (2002).
5. J. E. Borovsky, M. H. Denton, *Geophys. Res. Lett.* **33**, L20101 (2006).
6. J. E. Borovsky, M. Hesse, *Phys. Plasmas* **14**, 102309 (2007).
7. B. M. Walsh, D. G. Sibeck, Y. Nishimura, V. Angelopoulos, *J. Geophys. Res.* **118**, 4844–4851 (2013).
8. J. E. Borovsky, M. H. Denton, R. E. Denton, V. K. Jordanova, J. Krall, *J. Geophys. Res.* **118**, 5695–5719 (2013).
9. P. A. Cassak, M. A. Shay, *Phys. Plasmas* **14**, 102114 (2007).
10. J. Birn, J. E. Borovsky, M. Hesse, *Phys. Plasmas* **15**, 032101 (2008).
11. J. C. Foster, *J. Geophys. Res.* **98**, 1675 (1993).
12. J. C. Foster *et al.*, *J. Geophys. Res.* **110**, A09S31 (2005).
13. Q. H. Zhang *et al.*, *Science* **339**, 1597–1600 (2013).
14. M. Lockwood, H. C. Carlson Jr., *Geophys. Res. Lett.* **19**, 1731–1734 (1992).
15. V. Angelopoulos, *Space Sci. Rev.* **141**, 5–34 (2008).
16. See supplementary materials on *Science* Online.
17. G. Paschmann *et al.*, *J. Geophys. Res.* **91**, 11099 (1986).
18. A. L. La Belle-Hamer, A. Otto, L. C. Lee, *J. Geophys. Res.* **100**, 11875 (1995).
19. C. T. Russell, R. C. Elphic, *Space Sci. Rev.* **22**, 681 (1978).
20. L. C. Lee, Z. F. Fu, *Geophys. Res. Lett.* **12**, 105–108 (1985).
21. J.-H. Shue *et al.*, *J. Geophys. Res.* **102**, 9497 (1997).
22. P. T. Newell *et al.*, *Ann. Geophys.* **20**, 1039–1047 (2002).

Acknowledgments: Supported by NSF grant AGS-1136827. We acknowledge NASA contract NAS5-02099 and instrument teams for use of the data from the THEMIS Mission, specifically the ESA, EFI, and FGM teams. Work at MIT Haystack Observatory was supported by NSF Cooperative Agreement AGS-1242204.

Supplementary Materials

www.sciencemag.org/content/343/6175/1122/suppl/DC1
Supplementary Text
Table S1
References (*23*–*26*)

15 October 2013; accepted 6 February 2014
10.1126/science.1247212

Tunable Phonon Polaritons in Atomically Thin van der Waals Crystals of Boron Nitride

S. Dai,[1] Z. Fei,[1] Q. Ma,[2] A. S. Rodin,[3] M. Wagner,[1] A. S. McLeod,[1] M. K. Liu,[1] W. Gannett,[4,5] W. Regan,[4,5] K. Watanabe,[6] T. Taniguchi,[6] M. Thiemens,[7] G. Dominguez,[7,8] A. H. Castro Neto,[3,9] A. Zettl,[4,5,10] F. Keilmann,[11] P. Jarillo-Herrero,[2] M. M. Fogler,[1] D. N. Basov[1]*

van der Waals heterostructures assembled from atomically thin crystalline layers of diverse two-dimensional solids are emerging as a new paradigm in the physics of materials. We used infrared nanoimaging to study the properties of surface phonon polaritons in a representative van der Waals crystal, hexagonal boron nitride. We launched, detected, and imaged the polaritonic waves in real space and altered their wavelength by varying the number of crystal layers in our specimens. The measured dispersion of polaritonic waves was shown to be governed by the crystal thickness according to a scaling law that persists down to a few atomic layers. Our results are likely to hold true in other polar van der Waals crystals and may lead to new functionalities.

Layered van der Waals (vdW) crystals consist of individual atomic planes weakly coupled by vdW interaction, similar to graphene monolayers in bulk graphite (*1*–*3*). These materials can harbor superconductivity (*2*) and ferromagnetism (*4*) with high transition

Simultaneous Ground- and Space-Based Observations of the Plasmaspheric Plume and Reconnection

B. M. Walsh *et al.*

Science **343**, 1122 (2014);
DOI: 10.1126/science.1247212